Low-power, small-form-factor angle sensing circuit for an electrostatic, quasi-static MEMS mirror in AR applications

Sangtak Park[1,a], Matthew Wakelin[a], Daniel Malea[a], Bergen Fletcher[a]
[a]Google Canada, 24 Charles St. West, Kitchener, Ontario, N2G 1H2, Canada

ABSTRACT

This paper presents a new, low-voltage, and small-form-factor analog front-end (AFE) circuit that measures the torsional angle of an electrostatically-actuated, quasi-static MEMS mirror, while it operates at a frame rate of 50 Hz to 60 Hz or higher, following a given angle profile, such as a sawtooth or triangle profile. The quasi-static MEMS mirror is actuated with a pair of two high-voltage (HV) differential signals. To enforce this quasi-static MEMS mirror to track a given angle profile or trajectory with minimum error, this MEMS mirror is driven by feedback control that requires a sensor capable of measuring its mechanical or optical angle in real time with high enough bandwidth and sensitivity. Hence, we design and implement the angle sensing circuit (ASC) that meets the low-power, low-cost, and small-form-factor requirements to reduce power consumption, size, and weight for AR applications. This ASC consists of a variable gain amplifier (VGA) and an envelope detector that operates at 3.3 V and draws about 1 mA during operation.

Keywords: Angle sensing circuit, Capacitive angle sensing, electrostatic and quasi-static MEMS mirror, Variable gain amplifier (VGA), Laser Beam Scanning (LBS), AR glasses, AR applications

1. INTRODUCTION

In recent years, a scanning MEMS mirror has found its applications in automotive, commercial, medical, and industrial markets, such as LiDAR[1,10] (Light Detection And Ranging), a pico projector[2,9,22], NED[3,9,20,21] (Near Eye Display) for AR glasses, eye tracking[4], OCR[5] (Optical Coherence Tomography), and 3D printing based on 2PP[7] (Two Photon Polymerization), to name a few, whether it is made of a single dual-axis MEMS mirror[8,9,10,22] or two single-axis MEMS mirrors[9,10,22], as shown in Fig. 1. It has been also fabricated with different technologies[9,10,22] and operating within different physics[9,10,22]; most popular types are, for instance, electromagnetic[9,10], electrostatic[8,9,10], piezoelectric[9,10], and electrothermal[11,12]. Many MEMS transducers, except for electrostatic one, have a piezoresistive or piezoelectric sensor[9,10] on their supporting structure as an embedded sensor to measure their displacement, while either capacitive sensing[9,10] or motion-induced current[13] is the most prominent sensing method in electrostatic MEMS sensors and actuators that vary their capacitance during their bending or torsional motion. However, its motion-induced current[13] is proportional to its velocity or angular velocity, not angular displacement. Hence, a state estimator might be required to compute its angle from the measured angular velocity, while the capacitive sensing could directly measure its angle in real time. There are many capacitive sensing methods[9,10] proposed over the years. But most of them are not optimized in terms of size, weight, form factor, power consumption, and cost for AR applications. Hence we design and build the new, low-power, and small-form-factor angle sensing circuit (ASC) that capacitively measures the mechanical angle of the quasi-static MEMS mirror presented in Fig. 1 and Fig. 2. The ASC studied in this paper is made of a variable gain amplifier (VGA) and an envelope detector, while drawing about 1 mA at 3.3 V during its normal operation: The output of VGA is modulated, proportional to the ratio of two MEMS capacitances; and the envelope detector demodulates the output of VGA, extracting its envelope proportional to the torsional angle of the quasi-static MEMS mirror.

[1] sangtak@google.com; tel.: 1-519-513-3334 (office); www.google.com

This paper focuses on an electrostatically-actuated, quasi-static MEMS mirror operating at a frame rate of 50 Hz to 60 Hz and its small, low-power angle sensing circuitry (ASC) in AR applications. Since an underdamped, quasi-static MEMS mirror is driven to follow a given angle profile at a frame rate, its motion could be controlled via either feed-forward (input shaping[14,15]), feedback control, or a combination of both. The input shaping might be the best way to control its motion with prior knowledge of its dynamics, such as its resonance and quality factor or damping, as long as these parameters do not vary over temperature and time. However, even with prior knowledge of its dynamics, its start-up time could be quite long, because we have to wait for its transients to die out. Hence, to reduce its start-up time and make it more robust to its parameter variations and external disturbance, feedback control is implemented to drive this underdamped, quasi-static MEMS mirror, which requires a sensor that measures its angle in real time. Hence, we design and implement the ASC that capacitively measures its torsional angle. Moreover, ASC is designed and optimized, considering the following requirements for AR applications: low power, small form factor, low mass, and low cost, so as to reduce power consumption, size, and weight.

Fig. 1a Optical pictures of electrostatically-actuated, quasi-static (left) and resonant (right) MEMS mirrors fabricated by ST Microelectronics[2,17] (STM) and made of two wafers[2]: A top structural wafer and a bottom handling wafer. (courtesy of STM)

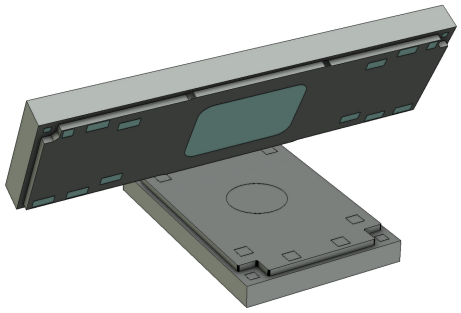

Fig. 1b One opto-mechanical configuration of LBS[18-20] (laser beam scanning) based on two single-axis MEMS mirrors: the resonant MEMS mirror is located at the bottom and the quasi-static MEMS mirror is positioned at the top.

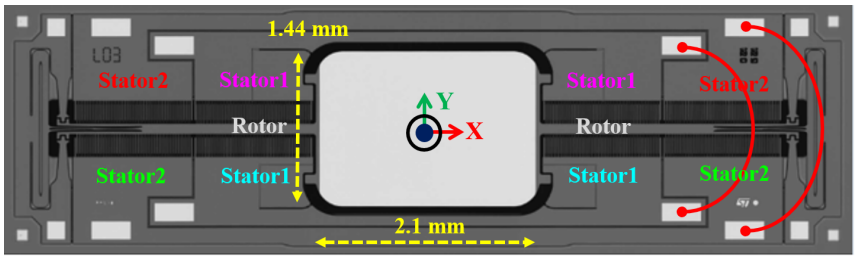

Fig. 2a Top view of the quasi-static MEMS mirror that shows its mirror plate structurally supported by two torsion bars and its staggered vertical comb (SVC) fingers on both rotors and stators: Its four inner stators (Stator 1) are electrically connected together and used to rotate its mirror plate clockwise (CW) along the x axis; and its four outer stators (Stator 2) are also electrically connected and used to rotate its mirror plate counter-clockwise (CCW) along the x axis, while avoiding its spurious out-of-plane bending (piston) motion.

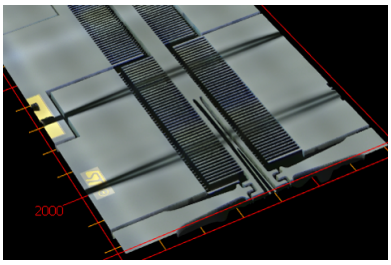

Fig. 2b SEM of the right side of the quasi-static MEMS mirror showing the mechanical torsion bar, SVC[16], two mechanical stoppers, and two bonding wires electrically connecting the upper stators and the lower stators.

2. QUASI-STATIC MEMS MIRROR

As presented in Fig. 1b, the raster scanning could be achieved by a pair of two single-axis MEMS mirrors; the resonant MEMS mirror generates two raster scan lines per period, while the quasi-static MEMS mirror rotates at a frame rate in an orthogonal direction to the scanning direction of the resonant MEMS mirror at its torsional resonance ranging from 20 kHz to 30 kHz, away from human audible spectrum. The optical image of the quasi-static MEMS mirror with staggered vertical comb[16] (SVC) fingers is shown in Fig. 2a, while the SEM of its right side is presented in Fig. 2b. It is made of two wafers: a top structural wafer and a bottom handling wafer, and its detailed fabrication process can be found in (2).

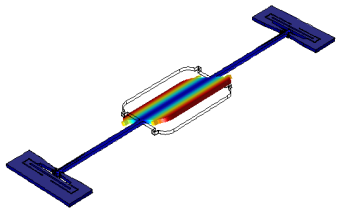

Fig. 3a Primary torsional motion at 625 Hz determined from its FEM

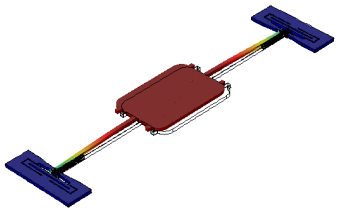

Fig. 3b Spurious in-plane bending motion at 1.2 kHz

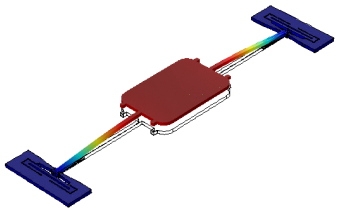

Fig. 3c Out-of-plane bending (piston) motion at 2.1 kHz

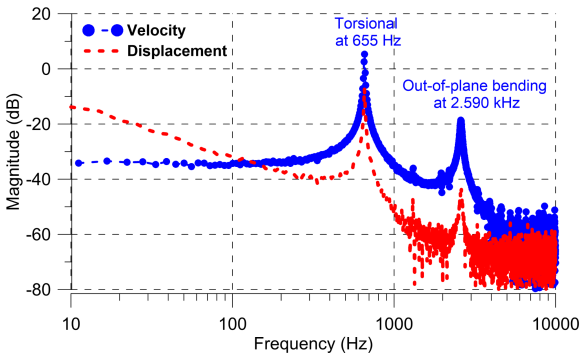

Fig. 4a The 1st torsional and the 3rd out-of-plane bending (piston) modes are measured at 655 Hz and 2.59 kHz; the blue circles and red-dashed lines represent velocity and displacement measurements with LDV, respectively.

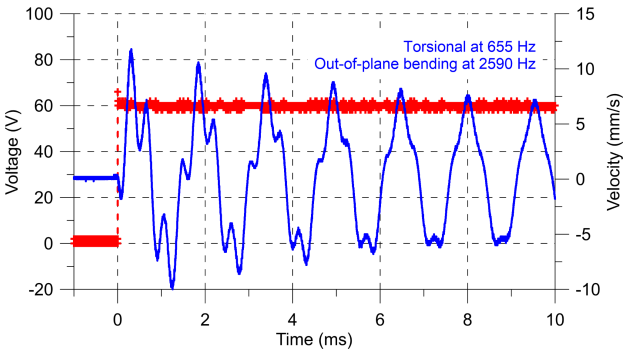

Fig. 4b Step response of the quasi-static MEMS mirror, when the 60 V step input is applied to one of its stators; the ring-down and the half-power bandwidth methods are used to determine its quality factors: 81 for its torsional motion and 23.5 for its out-of-plane bending motion.

First, the eigenvalue analysis is performed with its Finite Element Model (FEM) in COMSOL® to determine its resonances and mode shapes, as presented in Fig. 3. Then, we measure its resonance and corresponding mode shapes with LDV, as shown in Fig. 4. Its 1st torsional resonance is estimated to be 625 Hz and measured at 655 Hz, and its 3rd out-of-plane bending (piston) mode shape is estimated to be 2.1 kHz and measured at 2.59 kHz in Fig. 4. We also use the ring-down method with logarithmic decrement and the half-power bandwidth method to determine the quality factors of its torsional motion and out-of-plane

bending (piston) motion, which are measured to be 81 and 23.5, respectively, although the nonlinear squeeze-film damping will further reduce its quality factors with bigger opening angles.

Unlike the resonant MEMS mirror, the quasi-static MEMS mirror is driven by a pair of HV differential signals applied to Stator 1 and Stator 2, respectively, while its rotor is biased at 1 V DC. Its equation of motion in a canonical form is derived and presented in Eq. 1. The MEMS capacitances between its rotor and stators are also determined from its FEM at discrete angles in Fig. 5a, and the partial derivatives of the MEMS capacitance with respect to its torsional angle are derived from interpolation in Fig. 5b.

$$\ddot{\theta}(t) + \frac{\omega_0}{Q}\dot{\theta}(t) + {\omega_0}^2\theta(t) = \frac{1}{2J}\left(\frac{\partial C_1(\theta)}{\partial\theta}{V_{st1}}^2 + \frac{\partial C_2(\theta)}{\partial\theta}{V_{st2}}^2\right) \quad (1)$$

where θ, ω_0, Q, J, i, C_1, V_{st1}, C_2, and V_{st2} represent the angle in radian, the torsional resonance, the quality factor, the moment of inertia, the MEMS capacitance between its rotor and Stator 1, one of HV differential actuation voltage, the MEMS capacitance between its rotor and Stator 2, and the other HV differential actuation signal, respectively.

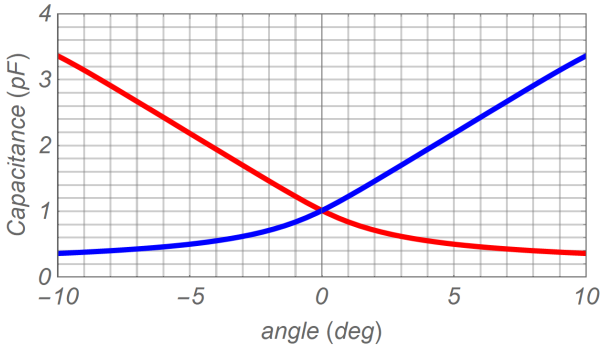

Fig. 5a MEMS Capacitances vs its torsional angle: The red and blue lines represent MEMS capacitances between its rotor and inner stators, as well as its rotor and outer stators, respectively.

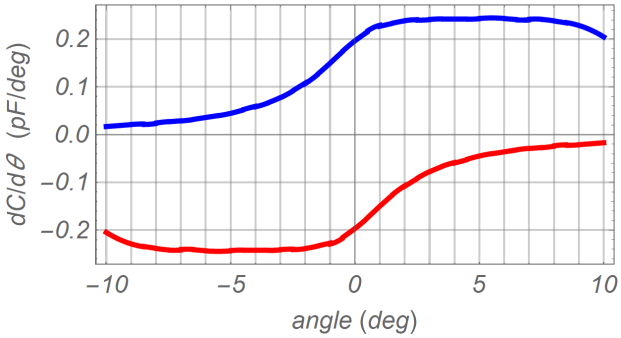

Fig. 5b Partial derivatives of MEMS capacitances with respect to its torsional angle: the red and blue lines represent its partial derivatives of MEMS capacitances, respectively.

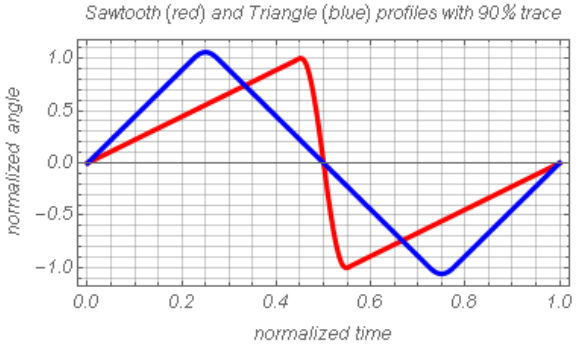

Fig. 6a Examples of the normalized angle profiles: A sawtooth profile (red) and a triangle profile (blue) with 90 % trace and 10 % retrace periods

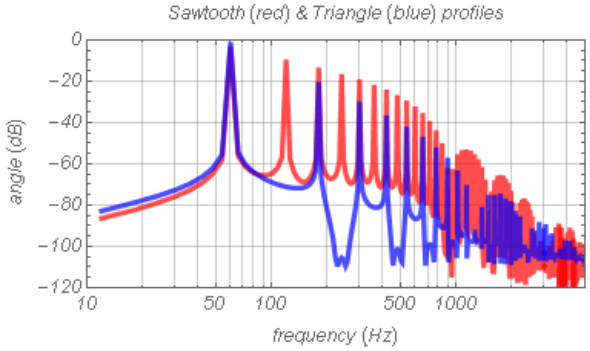

Fig. 6b Frequency components of the sawtooth (red) and triangle (blue) profiles with 90 % trace and 10 % retrace periods at a frame rate of 60 Hz

Although the quasi-static MEMS mirror and its electrostatic actuation are strongly nonlinear as presented in Eq. 1 and Fig. 5b, its HV differential actuation signals could be optimized in terms of linearity, lower voltage, or power consumption, for example, while driving the underdamped, quast-static MEMS mirror to follow a given angle profile, either sawtooth (red) or triangle (blue) profile in Fig. 6a. The sawtooth profile has a single 90 % trace period followed by a 10% retrace period in a single frame. The triangle profile consists of one 45% upward trace period, one 45 % downward trace period, and a 5 % retrace period right after each trace period in a single frame. Hence both the sawtooth and triangle profiles have the same amount of time to project the same number of raster scan lines in a single frame. However, the triangle profile is better suited for interlaced scans, while the sawtooth profile is better for progressive scans at the same frame rate. Furthermore, the triangle profile has less harmonics with smaller magnitudes than those of the sawtooth profile within the same operating conditions, such as the same opening angle and the same frame rate, as shown in Fig. 6b. The triangle profile has only the odd harmonics of the frame rate, 60 Hz, while the sawtooth profile has both odd and even harmonics with higher magnitudes. These higher harmonics of the sawtooth profile likely excite the torsional resonance of the quasi-static MEMS mirror, causing bigger ripples than the triangle profile does. In addition, the sawtooth profile requires higher angular velocity and acceleration during the retrace period, as shown in Fig. 7a. These higher angular velocity and angular acceleration lead to higher kinetic energy that has to be damped out or dissipated by higher control torque in Fig. 7b. In other words, the sawtooth profile requires more power and puts more load on feedback control, compared to the triangle profile.

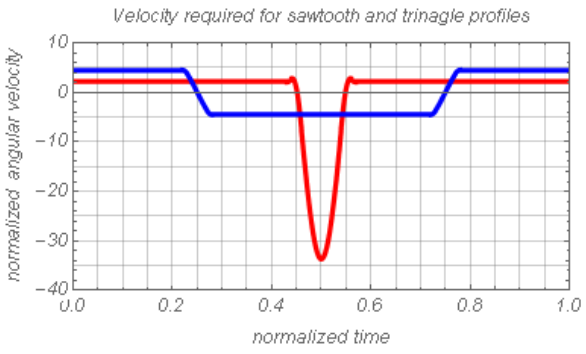

Fig. 7a Normalized angular velocity required to track the sawtooth (red) or triangle (blue) profile with 90 % trace and 10 % retrace periods in Fig. 6a.

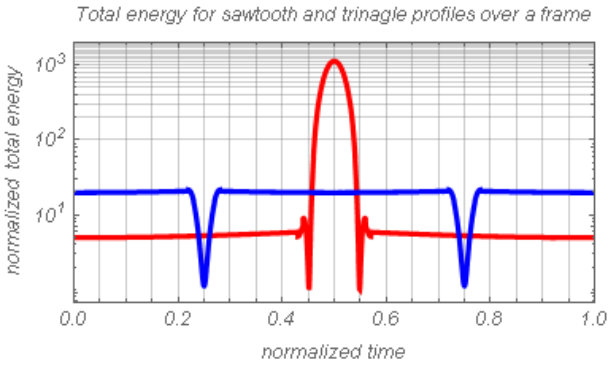

Fig. 7b Variations in total energy (the Hamiltonian) of the quasi-static MEMS mirror, while tracking the sawtooth (red) or triangle (blue) profile in Fig. 6a.

3. SENSING

To actuate or drive the quasi-static MEMS mirror at a frame rate, the differential pair of HV actuation signals are applied to its inner and outer stators, while its rotor is DC-biased at Vos, 1 V, through the DC feedback loop of VGA (U1) presented in Fig. 8. In addition, to measure the mechanical angle of the quasi-static MEMS mirror in real time, the low-voltage and high-frequency (LV & HF) excitation signal with 1.8 V at 1 MHz is injected to Stator 1 through the AC-coupling capacitor, Cs1, while the quasi-static MEMS mirror is driven by the high-voltage and low-frequency (HV & LF), differential pair of the actuation signals with max. 180 V at a frame rate of 60 Hz. This input configuration of VGA allows us to measure its mechanical angle in real time with the LV & HF excitation signal, while we drive the quasi-static MEMS mirror with its HV & LF actuation signals. Each pair of Rs1 and Cs1, as well as Rs2 and Cs2 work as bias tees providing separate DC (LF) and AC (HF) paths for HV & LF actuation and LV & HF excitation for sensing, respectively.

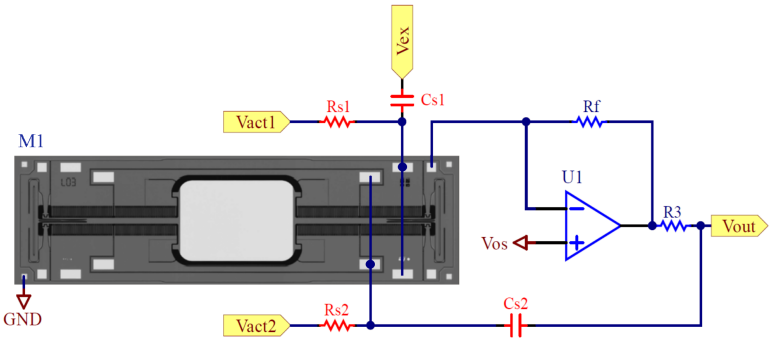

Fig. 8a Simplified circuit diagram showing the electrical connections to the quasi-static MEMS mirror (M1) for its sensing and actuation: Vact1 and Vact2 represent the differential pair of HV actuation signals (up to 180 V) at a frame rate of 60 Hz applied to both inner and outer stators, respectively; Vex represents the low-voltage (1.8 V), high frequency (1 MHz) excitation signal; Vout represents the output of the variable gain amplifier (VGA, U1); and Rs1, Rs2, Cs1, and Cs2 in red represent HV-rated passive components, while every other component operates at 3.3 V.

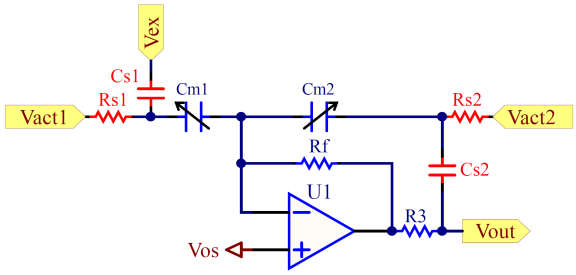

Fig. 8b Equivalent circuit diagram of the quasi-static MEMS mirror represented by two variable capacitors, Cm1 and Cm2, as well as electrical connections for HV & LF actuation signals (Vact1 and Vact2) and LV & HF carrier signal (Vex) injected to Stator 1 via the AC-coupling capacitor, Cs1. The output of VGA (Vout) is fed into an input of an envelope detector (not shown for clarity).

The simplified and the equivalent circuit diagrams in Fig. 8a and 8b present electrical connections for LV & HF sensing and HV & LF actuation of the quasi-static MEMS mirror. In Fig. 8a, its four inner stators and four outer stators are shown to be electrically connected together by two bonding wires presented in Fig. 2. Hence, its MEMS capacitances between its rotor & four outer stators and rotor & four inner stators could be lumped and modeled together as C_{m1} and C_{m2}, respectively. These two MEMS capacitances are the functions of its torsional angle and are shown in Fig. 5a, and its partial derivatives are also presented in Fig. 5b. Although parasitic capacitances due to bonding wires, substrates, and traces between PCB layers are not shown in Fig. 5 for clarity, the higher parasitic capacitances tend to lower the dynamic measurement range and sensitivity of ASC to the torsional angle of the quasi-static MEMS mirror. Hence, the parasitic capacitance has to be minimized during its PCB design, and both DC and AC feedback loops have to be physically as small as possible, in order to reduce cross-coupling or crosstalk. At DC or low frequency, the VGA in Fig. 8 acts as a voltage follower, setting its DC output voltage to be Vos, 1 V. At high frequency, the AC gain of the VGA varies, depending on both its MEMS capacitances and could be analyzed as in Eq. 2:

$$ACgain = \frac{(C_{p2} + C_{m2} + C_{s2})(C_{m1} + C_{p1})}{(C_{p1} + C_{m1} + C_{s1})(C_{m2} + C_{p2})} \approx \frac{(C_{m1} + C_{p1})}{(C_{m2} + C_{p2})} \quad (2)$$

where C_{p1}, C_{p2}, C_{s1}, C_{s2}, C_{m1}, and C_{m2} represent two parasitic capacitances in parallel with the MEMS capacitances (C_{m1} and C_{m2}), the two AC-coupling capacitors in series with MEMS capacitances, and two lumped MEMS capacitances, respectively.

Since two AC-coupling capacitors (C_{s1} and C_{s2}) are designed to be much bigger than the sum of the parasitic capacitance and the MEMS capacitances, the AC gain of the VGA would be simplified as in the right term of Eq. 2, where it is clearly shown that the two parasitic capacitances of the quasi-static MEMS mirror affect the gain of the VGA and the sensitivity to changes in the MEMS capacitances due to its torsional motion, as well as the linearity of the gain over its operating angles. However, we could still safely assume both parasitic capacitances to be constant and measure this gain over the operating (mechanical) angles from -5.5 ° to 5.5 ° during a calibration process to populate a look-up table (LUT). The two AC-coupling capacitors (C_{s1} and C_{s2}) might be adjusted to improve the gain linearity, but their max. capacitance has to be smaller or equal to the max. capacitive load that the HV amplifiers on the MEMS ASIC could drive in order to avoid instability. In addition, the pairs of R_{s1} & C_{s1} and R_{s2} & C_{s2} shall be HV-rated to prevent dielectric breakdown inside those components for safety and reliability.

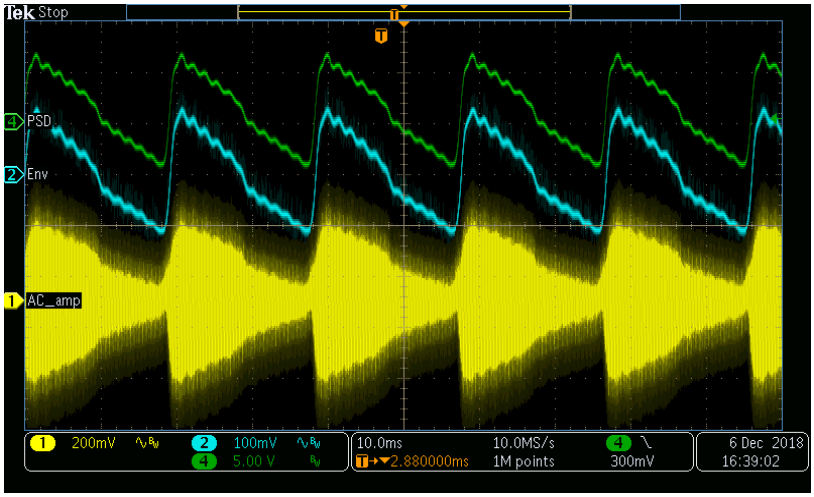

Fig. 9a Oscilloscope screenshot showing the output of VGA (CH1: yellow) modulated with its torsional angle, the demodulated output of the envelope detector (CH2: cyan), and the output of PSD (CH4: green, Position Sensing Device) representing the optically measured angle of the quasi-static MEMS mirror, while it is driven to follow a sawtooth profile with a jump in the middle from -5.5 ° to 5.5 °.

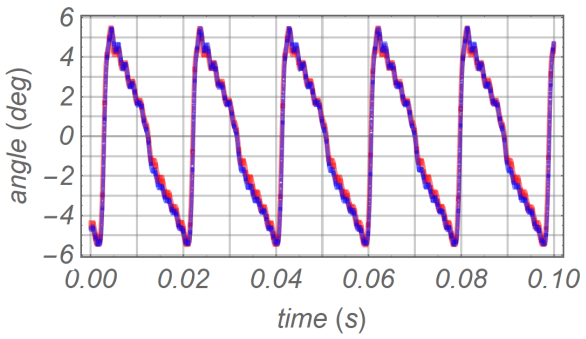

Fig. 9b Output of the ASC (blue) on top of the PSD measurements (red) after the ASC measurements are computed by averaging runs of 10 samples and scaled to fit.

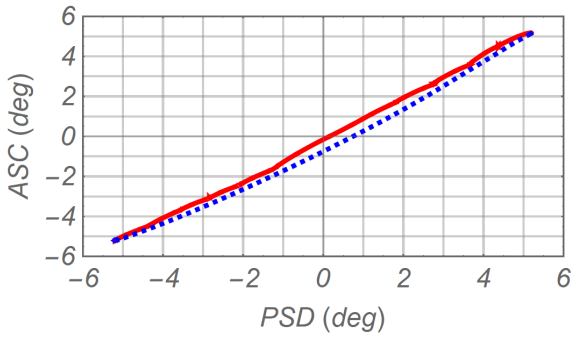

Fig. 9c Comparison of the ASC and PSD measurements; the hysteresis in the ASC measurements is caused by discrepancy in the ASC responses between the trace (red-solid) and retrace (blue-dashed) profiles.

The oscilloscope screenshot in Fig. 9a shows the modulated outputs of the VGA (CH1: yellow), the demodulated output of the envelope detector (CH2: cyan) and the output of the PSD optical measurement (Position Sensing Detector, CH4: green) with an amplifier (PSM2-10 and OT-301 from ON-TRAK), while the

quasi-static MEMS mirror is driven at a frame rate of 52.6 Hz without feedback control. Hence, its torsional resonant motion riding on top of the trace profiles could be seen on both outputs of the ASC and PSD in real time, and the PSD optical measurements are used as reference signals to analyze the signal integrity of the ASC measurements. Moreover, these high-frequency oscillations at its torsional resonance between 600 Hz and 700 Hz are called ripples, affecting the quality of a projected image within a frame. Hence, the ASC measures the mechanical angle of the quasi-static MEMS mirror and provides this measured angle to feedback control to reduce and eliminate these ripples. In Fig. 9b, the ASC measurements are computed by a moving average filter with 10 samples and scaled to fit with the PSD measurements with a constant gain, then are placed on top of the PSD measurements. Overall, both ASC and PSD measurements agree well with each other. However, the weak nonlinearity and hysteresis of the ASC measurements are also found and presented in Fig. 9c, where the red-solid and blue-dashed lines represent the angle measurement by the ASC during the trace and retrace periods, respectively. The SNR of the VGA is also determined with DFT of the time-series measurement data in Fig. 9a, and its frequency components via DFT are shown in Fig. 10a. Furthermore, the frequency responses of both the VGA and the envelope detector are also measured and presented in Fig. 10b.

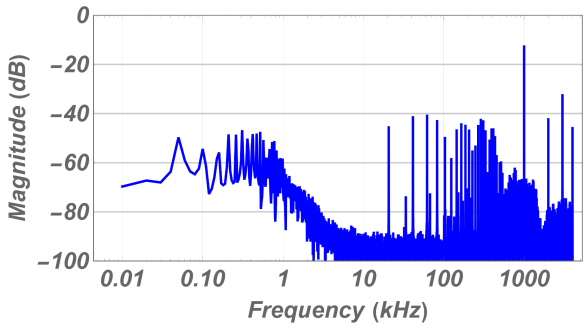

Fig. 10a Frequency components of the output of the VGA obtained from the time-series measurement data in Fig. 9a: the LV & HF carrier signal is at 1 MHz, and the SNR of VGA is determined to be about 60 dB.

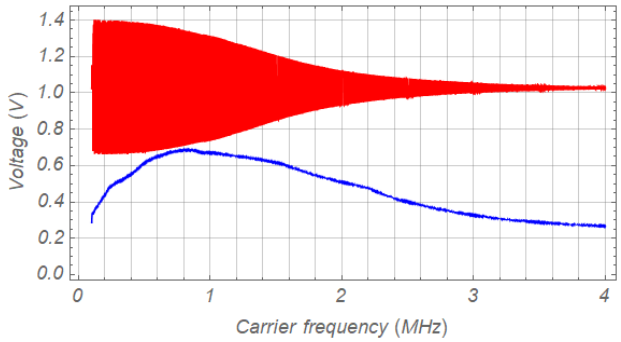

Fig. 10b Frequency responses of the VGA (red) and the envelope detector (blue) over a range of the carrier frequencies from 100 kHz to 4 MHz with the magnitude of 1.8 V_{pp}: the cutoff frequency of VGA is about 1 MHz, while the peak response of the envelope detector is around 800 kHz.

4. CONCLUSIONS

A quasi-static MEMS mirror in AR applications operates at a frame rate lower than its torsional resonance, following a sawtooth or triangle profile in a direction orthogonal to the scanning direction of a resonant MEMS mirror. Since the quasi-static MEMS mirror is underdamped, its resonant motion could be easily excited by every transition between traces and retraces or external disturbance, creating a number of bright and dark bands called ripples within a frame. In addition, these ripples could stretch and shrink portions of a projected image within a frame due to different angular velocity, degrading the quality of projected images. Hence we decided to use feedback control in order to make the quasi-static MEMS mirror more robust to ripples and external disturbance. Needless to say, the feedback control requires a sensor that measures its angle in real time, and consumes as little power as possible for AR applications. Hence, we design, implement, and validate the operation of the ASC with the quasi-static MEMS mirror that is driven with a pair of HV & LF differential actuation signals, while its angle is measured with the ASC and a single-ended LV & HF carrier signal. Finally, the feedback control with the ASC is implemented to drive the quasi-static

MEMS mirror to follow the sawtooth profile at a frame rate of 56.7 Hz, reducing its start-up time from min. 160 ms to max. 9.88 ms, as presented in Fig. 11.

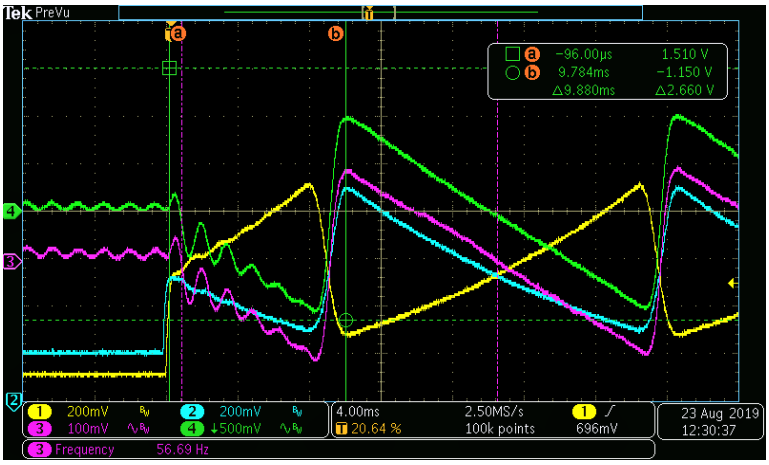

Fig. 11 Oscilloscope screenshot showing a pair of differential actuation signals (CH1: yellow & CH2: cyan) before amplification, the demodulated output of the ASC representing the torsional angle in real time (CH3: magenta) and PSD (CH4: green) during its start-up, while the quasi-static MEMS mirror is driven with the feedback control to track the sawtooth profile at a frame rate of 56.7 Hz; Its start-up time is reduced from min. 167 ms without feedback control to max. 9.88 ms with feedback control and ASC, respectively. (The Tabor 9400 HV amplifier with the gain of 50 is used to amplify the differential actuation signals to drive the quasi-static MEMS mirror.)

ACKNOWLEDGEMENT

The authors sincerely appreciate STM's technical support and advice regarding the fabrication of the electrostatic, resonant and quasi-static MEMS mirrors.

REFERENCE

[1] Wang, D., Thomas, L., Koppal, S., Ding, Y. and Xie, H., "A Low-Voltage, Low-Current, Digital-Driven MEMS Mirror for Low-Power LiDAR," IEEE Sens. Lett. 4(8), 1–4 (2020).

[2] Silva, G., Carpignano, F., Guerinoni, F., Costantini, S., De Fazio, M. and Merlo, S., "Optical Detection of the Electromechanical Response of MEMS Micromirrors Designed for Scanning Picoprojectors," IEEE J. Select. Topics Quantum Electron. 21(4), 147–156 (2015).

[3] Kim, M., Lee, S., Jo, Y., Lee, S. and Lee, B., "Compact tomographic near-eye display using a MEMS scanning mirror," Opt. Lett., OL 46(17), 4176–4179 (2021).

[4] Meyer, J., Schlebusch, T., Fuhl, W. and Kasneci, E., "A Novel Camera-Free Eye Tracking Sensor for Augmented Reality Based on Laser Scanning," IEEE Sensors J. 20(24), 15204–15212 (2020).

[5] Chen, Y., Hong, Y.-J., Makita, S. and Yasuno, Y., "Eye-motion-corrected optical coherence tomography angiography using Lissajous scanning," Biomed. Opt. Express, BOE 9(3), 1111–1129 (2018).

[6] Piyawattanametha, W., Cocker, E. D., Burns, L. D., Barretto, R. P. J., Jung, J. C., Ra, H., Solgaard, O. and Schnitzer, M. J., "In vivo brain imaging using a portable 2.9 g two-photon microscope based on a microelectromechanical systems scanning mirror," Opt. Lett., OL 34(15), 2309–2311 (2009).

[7] Pearre, B. W., Michas, C., Tsang, J.-M., Gardner, T. J. and Itchy, T. M., "Fast micron-scale 3D printing with a resonant-scanning two-photon microscope," Additive Manufacturing 30, 100887 (2019).

[8] Drabe, C., Kallweit, D., Dreyhaupt, A., Grahmann, J., Schenk, H. and Davis, W., "Bi-resonant scanning mirror with piezoresistive position sensor for WVGA laser projection systems," presented at SPIE MOEMS-MEMS, 9 February 2012, San Francisco, California, USA, 825209.

[9] Holmstrom, S. T. S., Baran, U. and Urey, H., "MEMS Laser Scanners: A Review," J. Microelectromech. Syst. 23(2), 259–275 (2014).

[10] Wang, D., Watkins, C. and Xie, H., "MEMS Mirrors for LiDAR: A Review," Micromachines 11(5), 456 (2020).

[11] Wang, P., Liu, Y., Wang, D., Liu, H., Liu, W. and Xie, H., “Stability Study of an Electrothermally-Actuated MEMS Mirror with Al/SiO2 Bimorphs,” Micromachines 10(10), 693 (2019).
[12] Zhou, L., Yu, X., Feng, P. X.-L., Li, J. and Xie, H., “A MEMS lens scanner based on serpentine electrothermal bimorph actuators for large axial tuning,” Opt. Express, OE 28(16), 23439–23453 (2020).
[13] Park, S., Khater, M., Effa, D., Abdel-Rahman, E. and Yavuz, M., “Detection of cyclic-fold bifurcation in electrostatic MEMS transducers by motion-induced current,” J. Micromech. Microeng. 27(8), 085007 (2017).
[14] Ngo, H.-Q.-T., Nguyen, Q.-C. and Kim, W.-H., “Implementation of input shaping control to reduce residual vibration in industrial network motion system,” 2015 15th International Conference on Control, Automation and Systems (ICCAS), 1693–1698, IEEE, Busan, Korea (South) (2015).
[15] Zuniga, N. S., Munoz, F., Marquez, M. A., Espinoza, E. S. and Carrillo, L. R. G., “Load transportation using single and multiple quadrotor aerial vehicles with swing load attenuation,” 2018 International Conference on Unmanned Aircraft Systems (ICUAS), 269–278, IEEE, Dallas, TX (2018).
[16] Hah, D., Patterson, P. R., Nguyen, H. D., Toshiyoshi, H. and Wu, M. C., “Theory and Experiments of Angular Vertical Comb-Drive Actuators for Scanning Micromirrors,” IEEE J. Select. Topics Quantum Electron. 10(3), 505–513 (2004).
[17] Guide, Step, “Laser Beam Scanning,” ST Microelectronics, <https://www.st.com/content/st_com/en/about/innovation---technology/laser-beam-scanning.html> (10 December 2021).
[18] Lee, B., Jo, Y., Yoo, D. and Lee, J., “Recent progresses of near-eye display for AR and VR,” Multimodal Sensing and Artificial Intelligence: Technologies and Applications II, S. Negahdaripour, E. Stella, D. Ceglarek, and C. Möller, Eds., 34, SPIE, Online Only, Germany (2021).
[19] Xiong, J., Hsiang, E.-L., He, Z., Zhan, T. and Wu, S.-T., “Augmented reality and virtual reality displays: emerging technologies and future perspectives,” Light Sci Appl 10(1), 216 (2021).
[20] Huikai Xie (Ed.)., [MEMS Mirrors.] (2018).